

Chapter 1

Introduction

1.1 Introduction

The aim of this study was to investigate the formation and dissociation of ionised molecules. The main focus of this thesis is the investigation of the dissociation of molecules with two positive charges, molecular dications. The development of a new apparatus to study the interactions of low energy electrons with molecules relevant to technological plasmas is also reported here.

1.2 Plasmas

Plasmas are partially or fully ionised gases that contain ions, electrons and possibly neutral atoms and/or molecules. They are found widely in nature, in stellar interiors, the interstellar medium and the Earth's ionosphere. Plasmas may be categorised into two types, thermal and non-thermal. In thermal plasmas, the energy required to generate ions and electrons is available from the thermal energy of the gas. High temperatures are required to ionise a significant proportion of the gas. Typical ionisation energies range from 9 to 15 eV. The temperatures required for kT to be equal to the atomic and molecular ionisation energies are over 100,000 K. These thermal plasmas generally exist in thermal equilibrium. Although very high temperatures are required for total ionisation of a gas, some thermal ionisation will occur in gases at lower temperatures. Non-thermal plasmas are not at thermal equilibrium, the energy required to ionise the gas is provided externally, for example, by the application of radio frequency fields or microwaves to accelerate the electrons in the gas. These accelerated electrons have enough energy to ionise the gas and have a much higher 'temperature' than that of the ions and neutral species within the plasma. Non-thermal, or technological, plasmas have a low degree of ionisation and so contain a large proportion of neutral species.

A major application of technological plasmas in industry is the etching of semiconductors. Current plasma techniques have been developed empirically, without computer simulation and modelling.¹ Therefore, the development of plasmas models and their constituent reactions is of interest to industry. Studies of

reactions in plasmas are required to supply cross-section and rate co-efficient data for the creation of a database of plasma processes¹. Many types of reactions occur within plasmas between the electrons, ions, neutral atoms and molecules. One of the areas of study required for inclusion in this database is the investigation of low energy electron-radical reactions.

1.3 Molecules in the Interstellar Medium

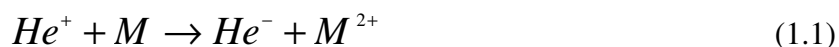
Many molecules have been found to exist within the interstellar medium.² The largest of those positively identified contain up to 13 atoms, such as HC₁₁N.³ Benzene has also been identified in the ISM.^{2,4}

It has been suggested that much larger molecules such as polyaromatic hydrocarbons, PAHs, and fullerenes, C₆₀ are also formed in the ISM and that these molecules are the source of emission and absorption bands, known respectively as the unidentified infrared, UIR, emission and diffuse interstellar bands.⁵ Allamandola *et al*⁶ have modelled UIR emissions with combinations of PAH spectra and suggested combinations of PAHs, which could exist in some interstellar regions.

It has been estimated that up to 50% of PAHs in the ISM are positively charged molecular ions.⁷ There is a proposal that some of these are ionised to give doubly charged ions, dications.⁷ The stability of dications is relevant to the investigation of their existence in the ISM, their chemical reactivity and their contributions to fragment ion populations.⁸

The formation of PAH dications, PAH²⁺, have been proposed to be formed by several methods, such as sequential ionisation and charge transfer. Leach⁷ proposed that the dications could be formed by a two-step ionisation by ultra-violet radiation from stars. The single and double ionisation appearance potentials have been studied for 21 PAHs and it was found that it could be possible for the two step ionisation process to occur for these molecules using photons of energy typically found in the

ISM.⁹ Another possible formation process could be double charge transfer from the interactions of He^+ , which is abundant in the ISM with the PAHs³; for example,



Two possible loss mechanisms have been suggested for PAH dications.^{7,8} The destruction of the dications could proceed in dense regions of the ISM via dissociative recombination.⁷ In less dense regions dications could fragment by coulomb explosion.⁸ The stability of dications is relevant to their expected lifetimes in less dense regions of the ISM.

The properties of molecular dications are also of interest for the modelling of planetary atmospheres. For example, CO_2^{2+} has been predicted to exist in the atmosphere of Mars.¹⁰

1.4 Molecular dications

Molecules with two positive charges, molecular dications, are generally thermodynamically unstable with respect to fragmentation into two singly charged fragments. The dissociation reaction of a general dication, AB^{2+} , is shown in equation (1.2).



Most dicationic molecular states fragment due to the coulombic repulsion. Chemical bonds within the dications can lead to some stability, shown schematically with the potential energy curve for AB^{2+} in figure 1.4.1, where $r_{\text{A-B}}$ represents the separation of the two fragment ions.

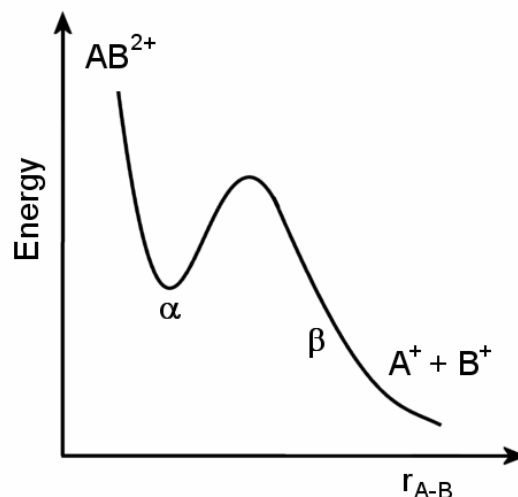


Figure 1.4.1 A schematic diagram of a potential energy surface for a molecular dication AB^{2+} , which dissociates into A^+ and B^+ fragments.

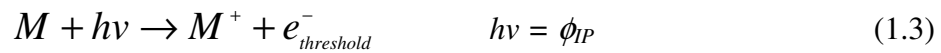
At large separations, indicated by β , coulombic repulsion dominates the potential energy curve, but for small separation, indicated by α , a potential well may be formed by the chemical bonds within the molecule. This potential well may support metastable states of the molecular dication with lifetimes up to minutes in length.

Theoretically calculated potential energy surfaces of molecular dications can give insight into their behaviour. Potential energy curves have been calculated for diatomic molecules, but for large molecules few theoretical studies have been performed. Large molecules have many more degrees of freedom and, therefore, multi-dimensional potential energy surfaces are required which investigate all possible motions of the molecule. Some calculations for dication potential energy surfaces for polyatomic molecules have been calculated, for example, carbon dioxide¹¹ and ethene.¹²

1.5 Molecular ion studies

1.5.1 Photoionisation

The absorption of a photon of energy, $E = h\nu$, by a molecule can result in photoionisation, the production of an ion and a free electron. If the photon energy is equal to the ionisation potential, $h\nu = \phi_{IP}$, an ion is produced in the ground state with the ejection of a threshold, or zero kinetic energy, electron;



If the photon energy is greater than the ionisation potential, $h\nu > \phi_{IP}$, then the additional energy, $h\nu - \phi_{IP}$, is shared between the ion and ejected electron. Therefore, the internal energy of an ion, $E(M^+)$, following single ionisation is given by equation (1.4) where $E(e^-)$ is the energy of the electron ejected in photoionisation.

$$E(M^+) = h\nu - \phi_{IP} - E(e^-) \quad (1.4)$$

The internal energy of the ion may be excited electronically or, in the case of a molecule, vibrationally and rotationally. If the energy of the electron can be measured experimentally then the energy of the ion can be determined. If only threshold electrons are detected then the internal energy of the ion is given by the energy of the photon and equation (1.4) becomes,

$$E(M^+) = h\nu - \phi_{IP} \quad (1.5)$$

There is also the possibility in ionisation processes that a super excited neutral state, M^* , is formed, which autoionises;



As the photon energy increases ions with greater internal energy may be formed. Double ionisation can occur when the photon energy is sufficient to release two electrons. Where the photon energy equals the double ionisation potential two threshold electrons are ejected.

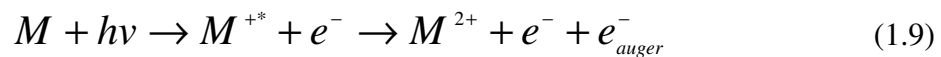


The energy of the doubly ionised molecule, is given by;

$$E(M^{2+}) = h\nu - \phi_{DIP} - E(e_1^-) - E(e_2^-) \quad (1.8)$$

Again, when the photon energy is greater than ϕ_{DIP} the excess energy is divided between the ion and the two emitted electrons. The two extreme cases being where the two electrons take away all the excess energy leaving a ground state dication and where two threshold, or zero energy, electrons are ejected leaving the molecular dication in an excited state.

If the photon energy is high enough a core electron may be ejected from the molecule. Core ionisation typically requires X-ray photons. The filling of the core hole following this ionisation can result in the emission of a second, Auger, electron. Equation (1.9) shows the process for the ejection of an Auger electron from a core excited ion, M^{+*} .



The kinetic energy of the Auger electron is then equal to the difference in the internal energy of the singly and doubly charged ions.¹³

1.5.2 Molecular ion spectroscopy

The properties of molecular ions can be determined following ionisation by observing the ejected electrons, the ion and some cases the ionising particle. Alternatively, molecular ions may be generated in an ion source and investigated, for example, in an ion beam experiment.

1.5.2.1 Photoelectron Spectroscopy

Photoelectron spectroscopy, PES,^{14,15,16} is the analysis of electrons emitted in photoionisation events. A fixed or variable energy light source is used to photoionise atoms or molecules and the emitted electrons are analysed with an electron monochromator or time-of-flight analyser.

In PES studies of single ionisation events the internal energy of an ion, $E(M^+)$, is given by equation (1.4), repeated below,

$$E(M^+) = h\nu - \phi_{IP} - E(e^-) \quad (1.4)$$

where $E(e^-)$ is the energy of the emitted electron, ϕ_{IP} is the ionisation energy and $h\nu$ is the photon energy. The electrons are emitted with a range of energies, which correspond to a variety of ionic states where $E(M^+) \leq h\nu - \phi_{IP}$. In threshold photoelectron spectroscopy, TPES, zero energy electrons are detected which correspond to ion states where $E(M^+) = h\nu - \phi_{IP}$. In this case the spectrum of molecular states is scanned by varying the photon energy.

An efficient method of collecting threshold electrons is with the Penetrating Field Technique, PFT.¹⁷ A weak electric field penetrates into the interaction region, where ionisation occurs, and extracts threshold electrons from 4π steradians. A shielded electrode creates a shallow saddle point potential, which guides threshold

electrons towards a detector. Higher energy electrons are not confined by the field and escape the interaction region. Some higher energy electrons do enter the detector from a small solid angle, but these can be removed with an energy analyser.

1.5.2.2 Zero kinetic energy spectroscopy

Zero kinetic energy, ZEKE, spectroscopy¹⁸ was developed as an improvement on TPES as a way of discriminating between threshold and near-threshold electrons. In this technique light from laser or synchrotron radiation sources is used to ionise the molecules under field free conditions. After a time delay a pulse is applied to extract electrons into an analyser/detector. The time delay allows the threshold electrons, with zero velocity, to be distinguished from the near-threshold electrons, with non-zero velocity. During the time delay, $\sim 1 \mu\text{s}$, the near-zero kinetic energy electrons move away from the threshold electrons. After the delay all electrons that remain in the source region are extracted into a time-of-flight analyser, the time-of-flight of the threshold and near-threshold electrons are distinct due to the difference in the initial position.¹⁸

Another method of obtaining ZEKE spectra for molecules is pulse field ionisation, PFI, of long lived Rydberg states of high principle quantum number, $n > 150$. The lifetimes of these highly excited Rydberg states can be $> 10 \mu\text{s}$. The electrons detected from the pulsed field ionisation of these states give the same information of the ionic states as electrons at or just above the threshold. High resolution spectra with resolved ro-vibrational structure can be observed with this method.¹⁹ Such high resolution is generally not achievable in PES or TPES.

1.5.2.3 Threshold photoelectrons coincidence

The threshold photoelectrons coincidence, TPEsCO, technique is a further development of the TPES for double photoionisation events where two electrons are

ejected. In double ionisation the internal energy of the ion, $E(M^{2+})$, is shown in equation (1.8), repeated below.

$$E(M^{2+}) = h\nu - \phi_{DIP} - E(e_1^-) - E(e_2^-) \quad (1.8)$$

Coincidences of pairs of threshold electron ejected in a double ionisation are detected whilst the photon energy is scanned. Again, ion states of energy $E(M^{2+}) = h\nu - \phi_{IP}$ are measured by the detection of threshold electrons, as the energy of the electrons is effectively zero.

One experimental TPEsCO configuration uses two electron energy analysers positioned on opposite sides of a source region to detect pairs of electrons.^{20,21} The penetrating field technique is used to guide threshold electrons into both of the analysers. The field guides threshold electrons equally to both detectors; an overlap of the two fields in the centre of the source region enables a high collection efficiency. In an alternative method,²² used in this study, all threshold electrons are drawn into a single electron energy analyser with a penetrating field and four detectors allow the measurement of coincidences between pairs of threshold electrons.

1.5.2.4 Time-of-flight photoelectron photoelectron coincidence

This new method of electron coincidence spectroscopy has been recently developed by Eland *et al*^{23, 24} to study double ionisation and doubly charged ions. In time-of-flight photoelectron photoelectron coincidence, TOF-PEPECO, electron pairs ejected in double photoionisation with all kinetic energies can be observed with magnetic bottle time-of-flight spectrometer. Photoelectrons are generated in photoionisation events using a pulsed noble gas light source. The electrons are then guided into the time-of-flight spectrometer by a magnetic mirror, which allows the extraction of electrons from almost 4π steradians of the source region. This spectrometer is 5.5 m long from source to detector; electrons are guided along the flight path by the magnetic field from a solenoid. In these experiments both electron

pair and single electron spectra are recorded. The electron pair spectrum is equivalent to TPEsCO spectrum, but for all electron pair energies.

1.5.2.5 Double charge transfer

Charge transfer experiments are an alternative way of investigating the ionic states of molecular ions. Fast moving charged ions interact with neutral molecules and electrons are transferred from the neutral to the ion. In double charge transfer, DCT, experiments²⁵ singly charged ions with several keV of translational energy capture two electrons from the neutral molecule to form a negative ion. The translational energy lost in the electron capture process gives a spectrum of the ionic states in the molecular dication.

During an electron capture collision the spin angular momentum of the pair of interacting atoms/molecules is conserved. The spin of the dication states formed in DCT can be selected by the choice of projectile ion. Generally ground state neutral molecules have zero spin angular momentum and are singlet. Typical incident ions are H^+ , OH^+ and F^+ , which become H^- , OH^- and F^- following double charge transfer. Both H^+ and H^- have zero spin angular momentum quantum number, so there is no change in spin and the dication formed must be of the same spin as the neutral. Therefore, singlet state dications are produced. By contrast, OH^+ has a triplet ground state and OH^- has a singlet ground state, in this case triplet states of the dication are excited in the interaction. Similarly, ground state F^+ is a triplet and ground state F^- is singlet, so again a triplet state is produced in the molecular ion.

1.6 Molecular ion dynamics

1.6.1 Photoelectron photoion coincidence

In Photoelectron photoion coincidence, PEPICO^{26,28,31} both the photoelectron and photoion formed in photoionisation events are detected. The initial state of the ion can be determined from the energy of the photoelectron. The stability or

fragmentation of the ionic state formed is observed by mass analysing the photoion. Two detectors are used to energy analyse the ions and electrons in coincidence.

This method has been modified for the detection of threshold photoelectrons in coincidence with photoions in the threshold photoelectron photoion coincidence experiments, TPEPICO.^{20,27} In single ionisation events where only one electron is ejected, this technique allows the energy of the monocation to be selected by the ionising photon energy. Again two analysers are used to detect the threshold electrons and ions. The threshold electrons only require a small draw-out field, whereas the ions require a much larger field. These experiments, therefore, generally use pulsing techniques to extract threshold electrons and ions from the source region; the detection of a threshold electron using a weak field triggers a strong field to extract ions into a mass analyser.²⁷

1.6.2 TPEsCO ion coincidences

This coincidence technique²² was developed to determine the stability and fragmentation dynamics of energy selected dications. The detection of pairs of threshold photoelectrons in coincidence with photoions from double ionisation events allows energy selection of the dications observed, as the internal energy of the dication is $E(M^+) = h\nu - \phi_{IP}$. The collection of fragment ion pairs formed in the dissociation of molecular dications along with the electron pairs in a four-particle, or quadruple, coincidence allows the investigation of the fragmentation dynamics of dications of known internal energy.

Quadruple coincidence measurements are made with a pulsing technique. The detection of pairs of electrons with the TPEsCO method triggers an extraction pulse that send ion into a time-of-flight mass spectrometer for mass selection and detection. Other coincidence measurements can be made, such as the detection of electron pairs with single ions, to give coincidences of electron pairs with dications.

1.6.3 True and false coincidences.

Various coincidence techniques have been used to study the dissociation of molecules where multiple fragment ions are detected. A complication of all coincidence techniques is that the results obtained contain a mixture of true and false coincidences. True coincidences are those where all particles detected originate from the same ionisation event. False coincidences also known as random or fortuitous are events where the particles detected do not originate from the same event. For example, in PEPICO experiments a true coincidence is where the detected photoelectron and photoion are generated in the same ionisation event. A false coincidence, in this example, is the detection of a photoelectron and photoion from two unrelated ionisation events.

Lowering the count rate of total coincidences can reduce the number of false coincidences obtained. False coincidences, however, are always present in the spectra and may be mathematically subtracted from experimental results. Mathematical methods for subtracting false coincidences from coincidence data have been described for various experimental techniques including PEPICO,²⁸ PEPIPICO²⁹ and for electron coincidences in (e, 3e) experiments.³⁰ The type of false coincidence and the mathematical subtraction methods depend on the data collection method in the experiment. In PEPICO experiments where electrons and ions are detected in coincidence, a static or pulsed field scheme can be used to extract ions from the source region. In these two different experiments the false coincidences contribute differently to the spectra.³¹

In static field experiments data are measured by 'time coincidence'. Ion and electrons flow continuously to the detectors and coincidences are determined by analysing the times-of-flight of the ions following the detection of an electron.^{28,31} In this case the false coincidences appear as a constant background signal in the time-of-flight spectrum. This constant background of false coincidences can be easily subtracted mathematically.^{28,31}

In pulsed field experiments²⁷ an ion extraction field is triggered by the detection of an electron, this causes all ions in the source region to be channelled into

the analyser at the same time and false coincidences are detected at the same time-of-flight as true coincidence. Therefore, both true and false coincidences are combined in the same time-of-flight peaks. The removal of false coincidences in this case is more complicated and requires further experimental data. A false coincidence spectrum can be recorded by using a random signal to trigger the ion extraction pulse. In this spectrum all ions detected are unrelated to the random trigger event; this gives a good estimate of the false coincidences, which need to be subtracted from the raw data.

The removal of false coincidences from triple coincidence data has been described by Frasinski *et al*²⁹ and Eland³² for PEPIPICO, where the time-of-flight of the two fragment ions are measured in coincidence with a photoelectron, and by Dupré for (e, 3e) experiments.³⁰ The analysis methods for PEPIPICO involve the measurement of extra spectra for subtraction from the raw data. Eland suggested the use of a PEPICO spectrum for the removal of false coincidences from PEPIPICO, the spectra being measured concurrently. In the method by Frasinski *et al*²⁹ the false coincidence were estimated by the collection of the photoion-photoion coincidence, PIPICO, spectrum. The PIPICO and PEPIPICO spectra could then be collated in a two dimensional matrix and the PIPICO subtracted from the PEPIPICO.

Long run times are required when collecting coincidence data where coincidence rates are low. This can cause problems where multiple spectra are required for data analysis as experimental conditions may change with time. For example, the false coincidence spectra may be recorded under slightly different experimental conditions and can cause inaccuracies in the subtraction process. Also the Poisson distribution of the electron triggers may not be the same as that of the random pulses that are used for the false spectra data collection. Powis *et al*³³ have suggested a technique for electron ion coincidences where both the standard and false spectra are measured concurrently and the electron start signal rate monitored so that the Poisson distributions of the electron and random triggers could be matched. This serves to increase the quality of false coincidence removal from the data.

In this study a method of removing false coincidences from quadruple coincidences of two electrons and two ions is presented using several extra spectra to estimate the false coincidence contributions in the raw data.³⁴ Most of the spectra recorded for the false coincidence removal were performed separately from the main data collection, but a new method of data collection was also used to collect data for all required spectra concurrently.

1.7 Electron - Molecule interactions

The interactions of molecules with other particles are of interest for modelling plasmas especially the interactions of neutral species with electrons and ions.

1.7.1 Electron scattering

There are two main types of electron scattering, elastic and inelastic. In elastic collisions none of the electrons kinetic energy is transferred to the internal energy of the molecule, whereas in inelastic collisions an excited molecule is generated by the transfer of kinetic energy from the electron to the internal energy of the molecule. The energy loss of the scattered electron can give information on the molecule, such as energy of electronic and vibrational levels.

In low energy scattering processes resonance structure may be present due to, for example, the formation of negative ion states by temporary attachment of the incident electron followed by auto-detachment,^{35,36}



The auto-detachment process can leave a ground state molecule, equivalent to elastic scattering, or an excited state molecule, M^* , which is equivalent to inelastic scattering.

1.7.2 Electron impact ionisation.

Collisions of high energy electrons and molecules can result in the ionisation of molecules,



This technique can be used to study ion states of molecular targets. An advantage of electron ionisation is that it can access states that are not excited in photoionisation studies, due to dipole forbidden transitions.³⁵

Electron ionisation is one of the dominant processes that occur in plasmas. One way of generating plasmas is by passing a high current discharge through a gas. Ions and electrons are generated via electron impact ionisation.

At high electron energies the electron impact dissociation may occur resulting in the fragmentation of the target molecule.



1.7.3 Dissociative electron attachment

In dissociative electron attachment, DEA, the attachment of an electron to a molecule creates a super excited state, or resonance, which then dissociates.^{35,37} This is shown in figure 1.5.1 and equation (1.13). The figure shows the attachment of an electron to a ground state molecule, AB , to form an anion in a repulsive electronic states, AB^{-*} , which then dissociates into fragments A^- and B .

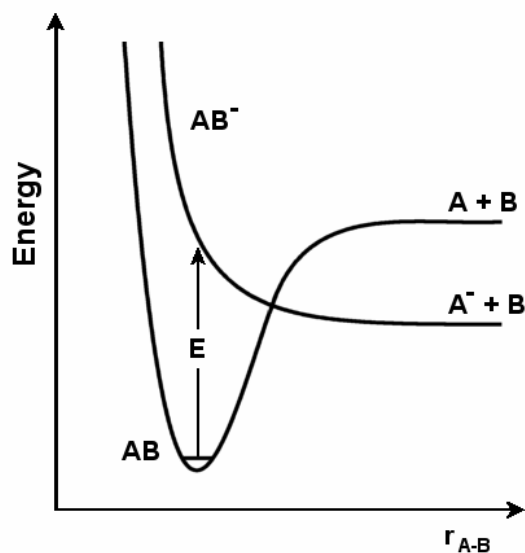
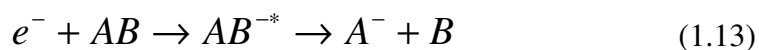


Figure 1.5.1 Potential energy curves for the dissociative electron attachment of an electron to a molecule AB .

The cross-sections for DEA are largest at low electron energies and are generally most significant for electron energies below 15 eV³⁷. The dissociation products are usually dependent on the energy of the attached electrons. For example, in the electron attachment to SF_6 , SF_6^{-} is formed for electron energies of 0.1 eV and below, whereas SF_5^{-} is formed with the attachment of up to ~ 1 eV electrons³⁸. By contrast, studies of the attachment of CCl_4 show the main dissociation product is Cl^{-} at low electron energies, < 2 eV³⁹.

Electron attachment may also occur by an indirect method. Energetic electrons may lose kinetic energy to inelastic collisions, these lower energy electrons can then attach to molecules such as SF_6 ³⁸.

1.8 Molecular dissociation

The dissociation dynamics of excited molecules and molecular dications is usually governed by the electronic or vibrational structure of the molecule, which can be represented with potential energy surfaces, PES. Generally, ground state molecules and ions exist in bound states and must acquire a certain energy to surmount a potential barrier to dissociate. If a molecule, AB , is excited into an unbound state, AB^* , shown in figure 1.8.1, the molecule will quickly dissociate.

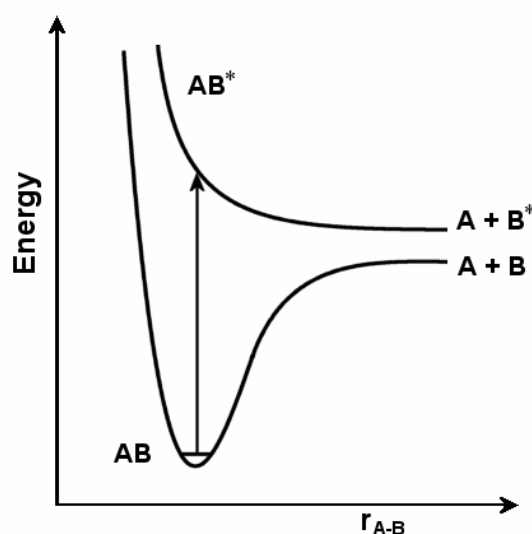


Figure 1.8.1 Dissociation of a molecule AB by excitation into an unbound state, r_{A-B} represents the separation of the fragments A and B .

Predissociation of a molecule occurs where an unbound state crosses a bound state below the ground state dissociation energy, figure 1.8.2. Therefore, if a molecule is excited into a vibrational state below the ground state dissociation energy, which is crossed by the unbound state, then dissociation may occur following the transfer of the molecule from the bound to the unbound state.⁴⁰ Therefore, dissociation occurs below the ground state dissociation energy.

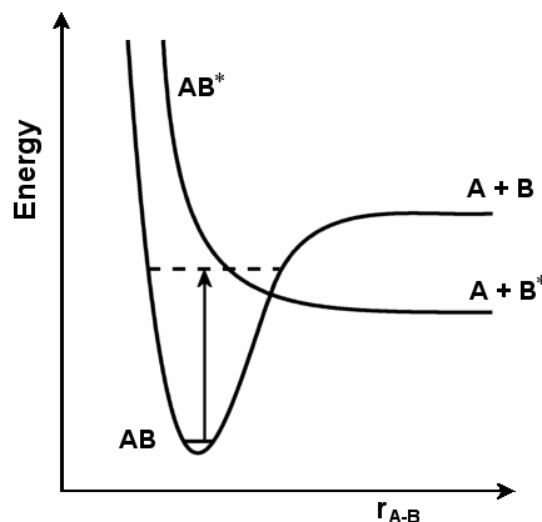


Figure 1.8.2 Predissociation of a molecule AB , where an unbound state crosses the bound ground state below the dissociation energy.

A molecule may rapidly dissociate if it has enough internal energy to overcome the ground state potential barrier. This is frequently not the case for large molecules with many modes of vibration, where the rate of dissociation can be slow for internal energies above the barrier height. This slow dissociation can be modelled with so called ‘statistical theory’ described in section 1.9.

Another possible decay mechanism for a molecule is that of quantum mechanical tunnelling of a fragment ion through the potential energy barrier. The rate of tunnelling decay is dependent on the width and height of the barrier and also the mass of the tunnelling particle; this is discussed for the case of tunnelling through a square potential barrier in section 1.10.

1.9 Unimolecular reaction theory

The rate of reaction of excited molecules has been considered previously in the theory of unimolecular reactions. The rate of unimolecular reactions is proportional to the number of reactant molecules and is, therefore, similar to radioactive decay. Several theories have been proposed to explain unimolecular

reactions from the early work of Lindemann to RRK and the more recent RRKM theory.

1.9.1 Lindemann theory

Lindemann theory^{41,42} describes the unimolecular reactions observed in the decay of molecules. The theory attempts to explain the rate of formation and decay of excited molecules, A^* , within a bath gas, M . Lindemann proposed that the dissociation followed a two step process, the first step being an activation step, where collisions of the molecule, A , within a bath gas produce molecules in excited states, A^* . The second step is then the dissociation of the excited molecule. The activation step involves an equilibrium reaction where both the excitation and de-excitation of molecules occur due to collisions within a gas. This is shown in equation (1.14), where the rates of excitation and de-excitation are k_1 and k_{-1} , respectively.



The reaction rates in this step are proportional to the number of collisions and are therefore pressure dependent. Products, P , are produced from the dissociation of A^* with a rate of k_2 , equation (1.15).



The rate of formation of the products, P , is proportional to the concentration of the excited molecules, $[A^*]$, and the rate at which they decay, k_2 ,

$$\frac{d[P]}{dt} = k_2[A^*] \quad (1.16)$$

The concentration of excited molecules can be determined by considering all processes that add to and subtract from the concentration of A^* and the rates at which they proceed, equation (1.17).

$$\frac{d[A^*]}{dt} = k_1[A][M] - k_{-1}[A^*][M] - k_2[A^*] \quad (1.17)$$

The steady state approximation is used to determine $[A^*]$. This assumes that the rates k_1 and k_{-1} are much greater than k_2 and therefore the concentration of excited states remain constant, *i.e.* $d[A^*]/dt = 0$. Thus, equation (1.17) becomes,

$$[A^*] = \frac{k_1[A][M]}{(k_{-1}[M] + k_2)} \quad (1.18)$$

The rate of formation of products is then found using equations (1.16) and (1.18);

$$\frac{d[P]}{dt} = \frac{k_1 k_2 [A][M]}{(k_{-1}[M] + k_2)} \quad (1.19)$$

Therefore, Lindemann found that the rate of formation of products is proportional to the concentration of $[A]$ and that equation (1.19) can be written in terms of a single unimolecular rate constant, k_{uni} , as shown in equation (1.20).

$$\frac{d[P]}{dt} = k_{uni}[A^*] \quad \text{where} \quad k_{uni} = \frac{k_1 k_2 [M]}{(k_{-1}[M] + k_2)} \quad (1.20)$$

The Lindemann theory was found to give a general qualitative description of the unimolecular rate, but not good quantitative results when compared to experiment.⁴²

1.9.2 RRK theory

Further developments of Lindemanns theory were the inclusion of statistical and quantum mechanics to the unimolecular decay theory by Rice, Ramsperger and Kassel. This became known as RRK theory.^{41,43,44}

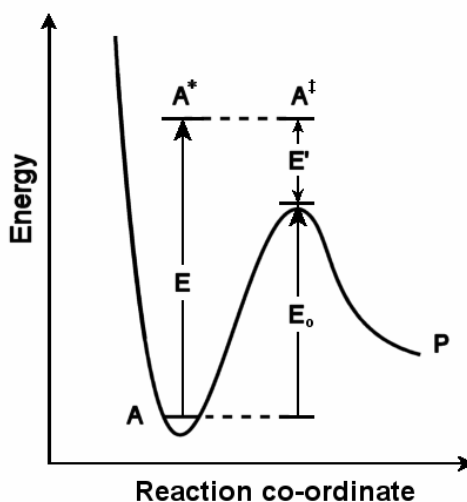


Figure 1.9.1 Statistical decay of an excited molecule A^* , with internal energy, E , over a barrier of height E_0 .

Where Lindemann theory includes no information on the molecules undergoing dissociation the updated models introduced the dependency of the rate of dissociation on the internal energy of the molecule. The main assumptions are that the dissociation involves one particular mode of vibrational motion within the molecule. For dissociation to occur a minimum amount of energy must be located in this key vibration. Therefore, if an excited molecule, A^* , has enough energy to dissociate it will not do so until the molecule is in a specifically excited state, A^\ddagger , where the sufficient energy is located in the mode of motion that leads to dissociation. This specifically excited state, A^\ddagger , is known as the transition state of the molecule. Once the transition state is formed then dissociation takes place with a rate k^\ddagger , to form dissociation products, P ;



The statistical decay of a molecule A over a potential barrier of height E_0 is shown schematically in figure 1.9.1 where the molecule has internal energy, E . The rate of dissociation of the transition state, k^\ddagger , is generally of the order of a vibrational frequency, 10^{14} s^{-1} . The rate of formation of molecules in the transition state, $d[A^\ddagger]/dt$, is shown in equation (1.22), where k_3 is the rate of the conversion of A^* to A^\ddagger .

$$\frac{d[A^\ddagger]}{dt} = k_3[A^*] - k^\ddagger[A^\ddagger] \quad (1.22)$$

The steady state approximation can be applied again as $k^\ddagger \ll k_3$ and $[A^\ddagger]$ is small, therefore, $d[A^\ddagger]/dt = 0$. The rate of conversion to the transition state, k_3 , is given by equation (1.23).

$$k_3 = \frac{k^\ddagger[A^\ddagger]}{[A^*]} \quad (1.23)$$

An assumption of this theory is that the internal energy of the molecule flows freely and randomly between the vibrational modes and dissociation only occurs when enough energy exists within the vibrational mode that leads to dissociation. Therefore, the probability of dissociation can be considered in terms of the number of ways of arranging the quanta of energy within the molecule. In the case of a polyatomic molecule it is assumed that a molecule contains s equivalent harmonic oscillators with frequency, ν . The value of s is given by the total number of degrees of freedom for the atoms in a molecule minus the number of translations and rotations, *i.e.* $3n - 6$ for a molecule with n atoms. If a molecule is provided with ν quanta of energy and a total of m is required in a particular mode for dissociation, then the probability of dissociation of the molecule can be determined by the ratio of the number of ways of arranging the ν quanta and $\nu - m$ quanta in the s oscillators,⁴¹ equation (1.24).

$$P_m^\nu = \frac{(\nu - m + s - 1)! \nu!}{(\nu - m)! (\nu + s - 1)!} \quad (1.24)$$

If the quantum numbers ν and m are much larger than s then the probability becomes,

$$P_m^\nu = \left(1 - \frac{m}{\nu}\right)^{s-1} \quad (1.25)$$

The internal energy of the molecule, E , and the minimum energy required for dissociation, E_o , can be expressed in terms of the quanta v and m , respectively, where $E_o = mh\nu$ and $E = vh\nu$. The probability of the energy, E_o , being located in the correct dissociation mode, out of a total energy, E , is given by,

$$P_{E_o}^E = \left(1 - \frac{E_o}{E}\right)^{s-1} \quad (1.26)$$

The probability of dissociation can be approximated as $[A^\ddagger]/[A^*]$, the ratio of the concentrations of molecules in the transition and excited states. Therefore, using equations (1.23) and (1.26) the rate of decay, k_3 can be found;

$$k_3(E) = k^\ddagger \left(1 - \frac{E_o}{E}\right)^{s-1} \quad (1.28)$$

Alternatively this can be written as shown in equation (1.29). Here the rate of decay can be seen to be dependent on the amount of excess energy, $E - E_o$, the molecule possesses, i.e. amount of energy above the dissociation barrier.

$$k_3(E) = k^\ddagger \left(\frac{E - E_o}{E}\right)^{s-1} \quad (1.29)$$

This theory gives a better quantitative agreement with experiment than Lindemann theory.⁴¹ RRK theory, however, tends to underestimate dissociation rates due to the approximations of the theory. Therefore, when fitting the theory to data the value of s must often be reduced by a factor of 2 – 5 for a good fit.^{43,46}

1.9.3 Further developments

Further developments of unimolecular theory give a more accurate interpretation of the molecular dissociation, but they require more detailed information on the molecules investigated. RRKM theory requires information on the transition states of the dissociating molecule to determine the rate of decay.^{41,42,44} The RRKM rate of decay of a molecule is,

$$k_3 = \frac{W(E')}{N(E)h} \quad (1.30)$$

where $N(E)$ is the density of states of the reactant molecule, E' is the energy remaining in the molecule above the dissociation barrier and $W(E')$ is the number of ways the energy, E' , can be arranged in the transition state.

Further developments of both RRK and RRKM have attempted to improve the theories by addressing some of the assumptions made by introducing anharmonicity⁴⁵ or a slower redistribution of energy in the molecule.⁴⁶

These advanced theories require additional details of the molecular structure and transition state of the dissociating molecule. This can be difficult to determine for large molecules where the structure of the transition state may not be the same as the ground state molecule and may also be dependent on the internal energy of the molecule.⁴⁷

1.9.4 Kinetic shift

In the previous sections the dependency of the rate of decay of a molecule on the internal energy of the system, has been discussed. The rate of statistical decay is, generally, lowest just above the dissociation barrier height, E_0 , and increases for

higher energies. Therefore, the lifetime, τ , of the molecule is greatest just above the barrier and decreases with increasing energy, as $\tau = 1/k$.

Experimental investigations of molecular lifetimes generally have a discrete observation time window, which corresponds to the length of time available for the observation of the decay distribution, as discussed in section 3.4. If the largest lifetime of the molecular system is not observable by the time window then the energy at which dissociation is first observed, the appearance energy, is not equal to the minimum dissociation energy, but is dependent on the observation time window. The difference in energy between the barrier height E_o and the observed appearance energy has been named the kinetic shift.^{47,48,49}

1.10 Tunnelling through a potential barrier

Another possible decay method for the dissociation of a molecule is that of tunnelling through a potential barrier. Where an excited state of a molecule is confined within a potential well there is a possibility that dissociation can occur via tunnelling of a fragment ion through the barrier. If a molecule is in an excited state, A^* , confined within a potential well of height, V_o , the transition state, A^\ddagger , may be formed by the tunnelling of a fragment ion through the potential barrier, as shown in figure 1.10.1. Once the transition state is formed it will quickly dissociate, with a rate k^\ddagger , to give products, P . The dissociation reaction is,



where k_i is the rate of tunnelling of the fragment through the potential barrier.

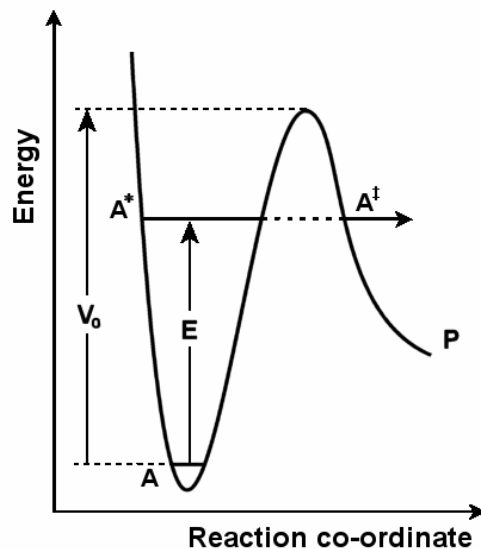


Figure 1.10.1 Schematic diagram of the tunnelling of a fragment of the molecule A^* through a barrier to produce a transition state molecule A^\ddagger , which rapidly dissociates to form products, P .

The rate of tunnelling may be approximated by considering the simplified case of a particle tunnelling through a square potential barrier.⁵⁰

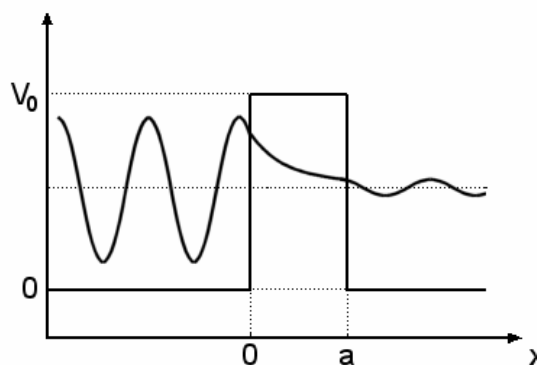


Figure 1.10.2 Schematic diagram of wave function, $\psi(x)$, tunnelling through a square potential barrier of width a and height V_0 (redrawn from reference 50).

The tunnelling of a particle with a wavefunction $\psi(x)$ through a square potential barrier is shown in figure 1.10.2. The wavefunction of the particle before, $x < 0$, within, $0 < x < a$, and after the barrier, $x > a$, can be represented by the following equations (see, for example, reference 50),

$$\psi_I = Ae^{ikx} + Be^{-ikx} \quad x < a \quad (1.32)$$

$$\psi_{II} = Ce^{\kappa x} + De^{-\kappa x} \quad 0 < x < a \quad (1.33)$$

$$\psi_{III} = Ee^{ikx} \quad x > a \quad (1.34)$$

$$\text{where } \kappa = \left(\frac{2m(E - V_0)}{\hbar^2} \right)^{1/2} \text{ and } k = \left(\frac{2mE}{\hbar^2} \right)^{1/2} \quad (1.35)$$

The coefficients of the above equations can be found by matching both the wavefunction and the derivatives of the wavefunctions at the boundaries of the barrier. The transmission coefficient, T , for the wavefunction is given by the ratio $|E|^2/|A|^2$ and is shown in equation (1.36).

$$T = \left[1 + \frac{V_0^2 \sinh^2(\kappa a)}{4E(V_0 - E)} \right]^{-1} \quad (1.36)$$

In the case of a high, thick potential barrier $\kappa a \gg 1$ the transmission coefficient can be approximated as,

$$T \approx \frac{16E(V_0 - E)}{V_0^2} e^{-2\kappa a} \quad (1.37)$$

The transmission coefficient can be approximated by the ratio k_i / k^\ddagger . Therefore, the rate of decay via a tunnelling mechanism through a barrier is,

$$k_i \approx \frac{16k^\ddagger E_i (V_0 - E_i)}{V_0^2} e^{-2\kappa a} \quad (1.38)$$

The rate of tunnelling is therefore dependent on the mass, m , of the tunnelling particle as κ is proportional to \sqrt{m} . The significance of this mass dependence is that for higher mass tunnelling will occur over shorter energy range.

1.11 Dissociation rates of molecules from single and multiple potential well systems

In the decay of large molecules there is a possibility of isomerisation occurring prior to dissociation. The competition of isomerisation and dissociation has been discussed previously in terms of multiple potential wells on potential energy surfaces.^{51,52} The dissociation rate of molecules with a multiple well system is explored here.

1.11.1 Single potential well

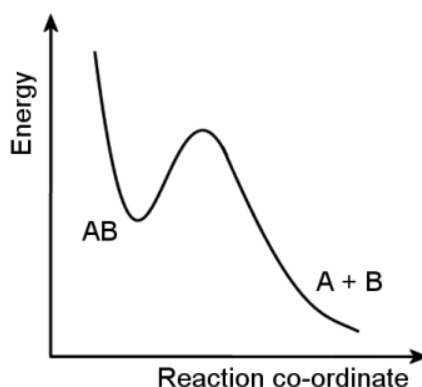


Figure 1.11.1 A schematic diagram of the potential energy surface of a dication AB with a single well.

The simplest potential energy surface for the dissociation of a molecule or a molecular ion is a single potential well, shown in figure 1.11.1.



Consider a molecule AB with fixed internal energy, which dissociates into fragments A and B with a rate constant k , equation (1.39). If the number of molecules which dissociate is N , then the rate of change of N is given by,

$$\frac{dN}{dt} = -kN \quad (1.40)$$

And therefore the number of fragment pairs produced after a time, t , is given by equation (1.41) where N_o is the number of undissociated dication at $t = 0$.

$$N(t) = N_o e^{-kt} \quad (1.41)$$

The rate of decay is related to the lifetime, τ as $k=1/\tau$. The probability of a dissociation, $P(t)$, occurring at a time, t , is proportional to $N(t)/N_o$ and therefore using equation (1.41) and determining a normalisation constant it is found that,

$$P(t) = \frac{1}{\tau} e^{-\frac{t}{\tau}} \quad (1.42)$$

1.11.2 Multiple potential well systems

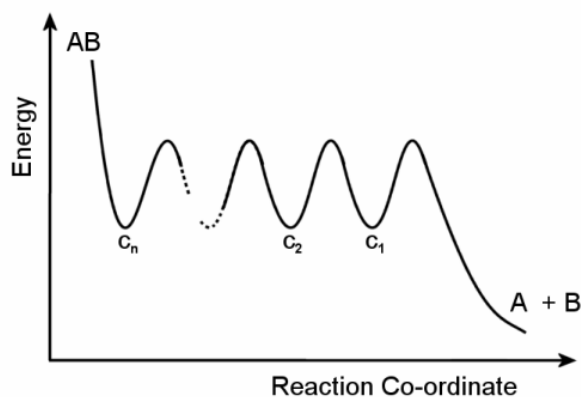


Figure 1.11.2 A schematic diagram of the potential energy surface of a dication AB , with multiple potential wells.

In a large molecule there is a possibility of isomerisation of the molecular structure prior to dissociation. Consider an idealised model system of n linked identical potential well systems, figure 1.11.2, where c_n is bounded by an infinite potential barrier and c_1 leads to the production of fragment pairs. It is assumed that the rate of isomerisation between any two wells, e.g. c_1 to c_2 , is equal to k and that the rate constant for the dissociation barrier is also k . The rate of formation of the

fragment pairs dN/dt is dependent on the number of particles in well c_1 and the decay rate of the barrier leading to dissociation, k .

$$\frac{dN}{dt} = -kc_1 \quad (1.43)$$

This result is similar to that found for the single well case. However, in the multiple potential well case the number of particles in c_1 is dependent on the isomerisation rates and number of particles in the other potential wells. This leads to a set of differential equations, which describes the dissociation of the molecule.

The two well system, as shown in 1.11.3, is considered here.

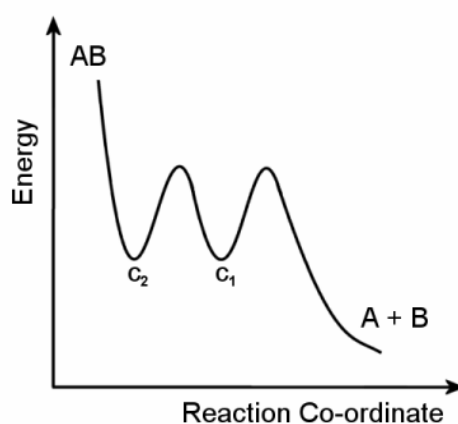


Figure 1.11.3 A schematic diagram of the potential energy surface of a dication AB , with two potential wells, c_1 and c_2 .

In this case the isomerisation and fragmentation reactions are shown in equations (1.44) and (1.45) respectively. It is assumed that all rates, k , are equal.



Differential equations for the change in c_1 and c_2 can be determined from the reactions;

$$\frac{dc_1}{dt} = kc_2 - 2kc_1 \quad (1.46)$$

$$\frac{dc_2}{dt} = kc_1 - 2kc_2 \quad (1.47)$$

These rates are found by considering all reactions, which add to or subtraction from the number of molecules in each well. If it is assumed that the content of each well, c_i , decays exponentially with a rate λ , then,

$$c_i = C_i e^{-\lambda t} \quad \text{and} \quad \frac{dc_i}{dt} = -\lambda C_i e^{-\lambda t} \quad (1.48)$$

Using these in equations (1.46) and (1.47) it is found that the equations can be reduced to a set of equations, (1.49), which can be solved to find the eigenvalues,

λ , for an eigenvector $\begin{pmatrix} C_1 \\ C_2 \end{pmatrix}$.

$$\begin{pmatrix} \lambda - 2k & k \\ k & \lambda - k \end{pmatrix} \begin{pmatrix} C_1 \\ C_2 \end{pmatrix} = 0 \quad (1.49)$$

Two eigenvalues, λ_I and λ_{II} , can be found by calculating the determinant of the 2x2 matrix;

$$\lambda_I = \frac{(3 + \sqrt{5})}{2} k \quad \text{and} \quad \lambda_{II} = \frac{(3 - \sqrt{5})}{2} k \quad (1.50)$$

The population of each well at a time t is given by the sum of the equation (1.48) for each eigenvalue found, as shown below,

$$c_1(t) = C_1(\lambda_I) e^{-\lambda_I t} + C_1(\lambda_{II}) e^{-\lambda_{II} t} \quad (1.51)$$

$$c_2(t) = C_2(\lambda_I) e^{-\lambda_I t} + C_2(\lambda_{II}) e^{-\lambda_{II} t} \quad (1.52)$$

Therefore, the total rate of decay for the molecule is dependent on two rates λ_I and λ_{II} , in this case, and cannot be modelled by a single exponential.

Generally for a multiple well system the population of a well, c_i , will be given by a sum of exponentials for each eigenvalue. For a n potential well system the population of any well, i , will be,

$$c_i(t) = \sum_{j=1}^n S_j C_i(\lambda_j) e^{-\lambda_j t} \quad (1.53)$$

where the S_j are a set of constants. Therefore, for an n -well system there will be n lifetimes and the dissociation will be dependent on a multiple exponential decay.

1.12 Dication lifetime studies

Several different experiments have been carried out to measure the lifetimes of dications.^{22,53,55-59} The different methods have different observation time windows, which is the period of time the experiment is sensitive dication fragmentation. Most of these techniques involve a flight region through which the dications travel with a certain time and may decay within. The lifetime determined is dependent on the length of this flight region and therefore the time window. The most common flight regions are time-of-flight mass spectrometers, storage rings or field free drift tubes.

In translational energy spectroscopy^{53,54} dications with several keV of kinetic energy are generated and mass selected. These then travel through a one metre long drift tube with a time window of $10^{-8} - 10^{-2}$ seconds. The lifetimes of the dications are determined from the distribution of the fragment ions formed in dissociations and compared with simulation.

Lifetimes over short time windows, a few nano-seconds, have been determined, for HeD^{2+} , by Ben-Itzhak *et al*⁵⁵ by using a strong permanent magnet to

deflect charged particles emitted from a dication source. The angle through which the ions are deflected depends upon their mass-to-charge ratio. The fragmentation of the dications within the magnetic field produces an angular spread of ions, which depend upon the time of dissociation. This angular spread can be modelled and the lifetime determined. The magnetic field is applied over ~ 1.6 cm and so this technique is only sensitive to very short lifetimes, \sim few nanoseconds.

The measurement of long lifetimes have been undertaken with ion storage rings.⁵⁶ Storage rings have time windows from microseconds to seconds. The upper limit corresponds to the length of time before the ion beam is destroyed by collision with the background gas, after ~ 10 s. The intensity of the neutrals that are ejected from the ring at a bending magnet of the storage ring is proportional to the number of dications stored in the ring. Therefore, the lifetime can be determined by measurements of the flux of neutrals. Lifetimes of dications, such as CO_2^{2+} , CO^{2+} and N_2^{2+} have been measured with this technique.⁵⁶

A method of lifetime determination has been developed by Bar-David *et al*⁵⁷ called the ‘foil-mesh’ method where it has been claimed that lifetimes longer than the time window can be calculated. In this method the flux of ions to a detector is monitored where the dications have a free flight path and where a thin foil is placed in trajectories of the ions. The foil serves to induce dissociation of the dications. The measurement without the foil gives the number of dications that undergo dissociation, whereas the measurement with the foil is used to determine the number of ion that reach the detector. A mean lifetime is determined by the normalised ratio of the two results. This method has been used to determine a lifetime of CD_2^{2+} , which is ~ 25 times longer than the observation time window.⁵⁷

Lifetimes of CO^{2+} dications with specific excited states was studied by measuring lifetimes for dications that dissociate with certain kinetic energy release⁵⁸ with 3D fragment imaging. Dications, generated by a van de Graaf generator and charge stripping, are velocity selected before entering a drift region. On detection, the positions of the fragments are measured with a CCD camera and the distance parallel to the beam is also measured by the difference in the time of arrival of the

two fragments. The state selection in this case comes from the measurement of fragment ions detected with a particular kinetic energy release, KER.

Time-of-flight mass spectrometry has also been used for a range of dication species including polyatomic molecules.⁵⁹ In these experiments the time window for lifetime determination is given by the time-of-flight of the parent dication in the mass spectrometer. Dications are created in photoionisation events and the dications and fragment ions detected in coincidence with electrons ejected in the ionisation events in a PEPICO type experiment called charged separation mass spectrometry, CSMS.⁵⁹ It was found that the dissociation of some of the dications investigated, were best described by more than one lifetime process.⁵⁹

The present work also uses time-of-flight mass spectrometry and coincidence techniques to determine lifetimes of the dications. A spectrometer is used as described by Penent *et al*²² to detect pairs of threshold electrons in coincidence with fragment ions. This has been used previously to investigate the dissociation and lifetime of CO²⁺. The detection of threshold electrons allows the initial energy of the dication to be selected by tuning the ionising photon energy. Therefore the fragmentation of ions of known internal energy can be monitored.

1.13 References

- ¹ National Research Council, *Database needs for modelling and simulation of plasma processing* (National Academy Press, Washington D.C., 1996)
- ² http://www.ph1.uni-koeln.de/vorhersagen/molecules/main_molecules.html,
Cologne database for molecular spectroscopy, November 2003
- ³ Petrie S., Bohme D., *Mon. Not. R. Astron. Soc.* **268** (1994) 103
- ⁴ Cernicharo J., Heras A.M., Tielens A.G.G.M., Pardo J.R., Herpin F., Guélin M., Waters L.B.F.M., *Astrophys. J.* **546** (2001) L123
- ⁵ Ehrenfreund P., Foing B.H., *Planet. Space. Sci.* **43** (1995) 1183
- ⁶ Allamandola L.J., Hudgins D.M., Sandford S.A., *Astrophys. J.* **511** (1999) L115
- ⁷ Leach S., *J. Electron. Spec. Rel. Phenom.* **41** (1986) 427
- ⁸ Millar T.J., Roueff E., Charnley S.B., Rodgers S.D., *Int. J. Mass Spectrom. Ion Proc.* **149/150** (1995) 389
- ⁹ Tobita S., Leach S., Jochims H.W., Rühl E., Illenberger E., Baumgärtel H., *Can. J. Phys.* **72** (1994) 1060
- ¹⁰ Witasse O., Dutuit O., Lilensten J., Thissen R., Zabka J., Alcaraz C., Bletly P.-L., Bougher S.W., Engel S., Andersen L.H., Seiersen K., *Geophys. Res. Lett.* **29** (2002) 1263
- ¹¹ Hochlaf M., Bennett F.R., Chambaud G., Posmus P., *J. Phys. B: Atom. Mol. Phys.* **31** (1998) 2163
- ¹² Ohrendorf E., Köppel H., Cederbaum L.S., Tarantelli F., Sgamellotti A., *J. Chem. Phys.* **91** (1989) 1734
- ¹³ Brehm J.J., Mullin W.J., *Introduction to the structure of matter* (Wiley, USA, 1989) p164
- ¹⁴ Turner D.W., Baker A.D., Brundle C.R., *Molecular Photoelectron Spectroscopy* (Wiley, London, 1970)
- ¹⁵ Carlson T.A. *Photoelectron and Auger spectroscopy* (Plenum, New York, 1975)
- ¹⁶ Eland J.H.D., *Photoelectron Spectroscopy* (Butterworths, London, 1984)
- ¹⁷ Cvejanović S., Read F.H., *J. Phys. B: Atom. Mol. Phys.* **7** (1974) 10
- ¹⁸ Schlag E.W., Peatman W.B., Müller-Dethlefs K., *J. Electron. Spec. Rel. Phenom.* **66** (1993) 139

-
- ¹⁹ Chewter L.A., Sander M., Müller-Dethlefs K., Schlag E.W., *J. Chem. Phys.* **86** (1987) 4737
- ²⁰ Hall R.I., McConkey A., Ellis K., Dawber G., Avaldi L., MacDonald M.A., King G.C., *Meas. Sci. Technol.* **3** (1992) 316
- ²¹ Hall R.I., Avaldi L., Dawber G., McConkey A.G., Ellis K., MacDonald M.A., King G.C., *Chem. Phys.* **187** (1994) 125
- ²² Penent F., Hall R.I., Panajotović R., Eland J.H.D., Chaplier G., Lablanquie P., *Phys. Rev. Lett.* **81** (1998) 3619
- ²³ Eland J.H.D., Vieuxmaire O., Kinugawa T., Lablanquie P., Hall R.I., Penent F., *Phys. Rev. Lett.* **90** (2003) 053003
- ²⁴ Eland J.H.D., Ho S.S.W., Worthington H.L., *Chem. Phys.* **290** (2003) 27
- ²⁵ Harris F.M., *Int. J. Mass Spectrom. Ion Proc.* **120** (1992) 1
- ²⁶ Danby C.J., Eland J.H.D., *Int. J. Mass Spectrom. Ion. Phys.* **8** (1972) 153
- ²⁷ Stockbauer R., *J. Chem. Phys.* **58** (1973) 3800
- ²⁸ Eland J.H.D., *Int. J. Mass Spectrom. Ion. Phys.* **8** (1972) 143
- ²⁹ Frasinski L.J., Stankiewicz M., Hatherly P.A., Codling K., *Meas. Sci. Technol.* **3** (1992) 1188
- ³⁰ Dupré C., Lahmam-Bennani A., Duguet A., *Meas. Sci. Technol.* **2** (1991) 327
- ³¹ Baer T., *Gas Phase Ion Chemistry* vol 1 ed M.T. Bowers (Academic Press, London, 1979) p153
- ³² Eland J.H.D., *Vacuum Ultraviolet Photoionization and Photodissociation of Molecules and Clusters* ed C. Y. Ng (World Scientific, Singapore, 1991)
- ³³ Powis I., Downie P., *Rev. Sci. Instrum.* **69** (1998) 3142
- ³⁴ Slattery A.E., Field T.A., Ahmad M., Hall R.I., Lablanquie P., Penent F., *Meas. Sci. Technol.* **13** (2002) 2007
- ³⁵ Mason N.J., Gingell J.M., Jones N.C., Kaminski L., *Phil. Trans. R. Soc. Lond. A* **357** (1999) 1175
- ³⁶ Gulley R.J., Lunt S.L., Ziesel J.-P., Field D., *J. Phys. B: At. Mol. Phys.* **31** (1998) 2735
- ³⁷ Klar D., Ruf M.-W., Hotop H., *Aust. J. Phys.* **45** (1992) 263
- ³⁸ Christophorou L.G., Olthoff J.K., *Int. J. Mass Spectrom.* **205** (2001) 27

- ³⁹ Matejcek S., Senn G., Scheier P., Kiendler A., Stamatovic A., Märk T.D., *J. Chem. Phys.* **107** (1997) 8955
- ⁴⁰ Banwell C.N., *Fundamentals of molecular spectroscopy* (McGraw-Hill, London, 1972) p222
- ⁴¹ Pilling M.J., Seakins P.W., *Reaction Kinetics* (Oxford University Press, GB, 1996) p121
- ⁴² Gilbert R.G., Smith S.C., *Theory of unimolecular and recombination reactions* (Blackwell scientific, GB, 1990)
- ⁴³ Ervin K.M., *Int. J. Mass Spectrom.* **195/196** (2000) 271
- ⁴⁴ Ervin K.M., *Chem. Rev.* **101** (2001) 391
- ⁴⁵ Song K. Hase W.L., *J. Chem. Phys.* **110** (1998) 6198
- ⁴⁶ Nordholm S., Bäck A., *Phys. Chem. Chem. Phys.* **3** (2001) 2289
- ⁴⁷ Baer T., *Adv. Chem. Phys.* **64** (1986) 111
- ⁴⁸ Chupka W.A. *J. Chem. Phys.* **30** (1959) 191
- ⁴⁹ Hickling R.D., Jennings K.R., *Org. Mass Spectrom.* **3** (1970) 1499
- ⁵⁰ Davies P.C.W., Betts D.S., *Quantum Mechanics* (Chapman and Hall, 2nd ed., GB, 1995) p49
- ⁵¹ Baer T., Brand W.A., Bunn T.L., Butler J.J., *Faraday Discuss. Chem. Soc.* **75** (1983) 45
- ⁵² Duffy L.M., Keister J.W., Baer T., *J. Phys. Chem.* **99** (1995) 17862
- ⁵³ Mathur D., *Nucl. Instr. Meth. Phys. Res. B* **99** (1995) 121
- ⁵⁴ Safvan C.P., Mathur D., *J. Phys. B: At. Mol. Phys.* **26** (1993) L793
- ⁵⁵ Ben-Itzhak I., Bouhnik J.P., Gertner I., Heber O., Rosner B., *Nucl. Instr. Meth. Phys. Res B* **99** (1995) 127
- ⁵⁶ Mathur D., Andersen L.H., Hvelplund P., Kella D., Safvan C.P., *J. Phys. B: At. Mol. Phys.* **28** (1995) 3415
- ⁵⁷ Bar-David A., Ben-Itzhak I., Bouhnik J.P., Gertner I., Levy Y., Rosner B., *Nucl. Instr. Meth. Phys. Res B* **160** (2000) 182
- ⁵⁸ Bouhnik J.P., Gertner I., Rosner B., Amitay Z., Heber O., Zajfman D., Sidky E. Y., Ben-Itzhak I., *Phys. Rev. A* **63** (2001) 032509
- ⁵⁹ Field T.A., Eland J.H.D., *Chem. Phys. Lett.* **211** (1993) 436

Chapter 2

Experimental procedure for TPEsCO ion coincidence

2.1 Introduction

Molecules with two positive charges, molecular dications, were investigated with the use of a TPEsCO ion coincidence spectrometer¹ to detect photoelectrons and ions in coincidence. This spectrometer comprised of an electron spectrometer and a time-of-flight mass spectrometer, which allowed the time-of-flight of the ions to be measured following the detection of pairs of photoelectrons. The molecular dications were formed by single photon double ionisation of neutral ground state molecules in the common source region of the two spectrometers. Coincidences were recorded between pairs of threshold photoelectrons and the fragment ions formed in the dissociation of the dications. The detection of the threshold photoelectron pairs, with the use of the threshold photoelectrons coincidence, TPEsCO, technique,² triggered an extraction pulse that pushed any ions within the source region into the time of flight, TOF, mass spectrometer. The times-of-flight of the ions following the extraction pulse were measured and recorded by an online computer.

In the study of molecular dication fragmentation it is desirable to know the state in which the dication exists prior to dissociation. This can be difficult to determine for large molecules, however, the internal energy of a molecule can be determined experimentally if all processes, which add or subtract energy from the molecule during the ionisation event are known. Equation (2.1) gives the internal energy, $E(M^{2+})$, of a molecular dication, M^{2+} , following a double ionisation event, where the molecule is supplied with energy $h\nu$ from the incident photon, ϕ_{DIP} is the double ionisation potential, the work done in ionising the molecule and $E(e_1)$ and $E(e_2)$ are the energies taken away by the ejected photoelectrons.

$$E(M^{2+}) = h\nu - \phi_{DIP} - E(e_1) - E(e_2) \quad (2.1)$$

In equation (2.1) the only experimentally unknown quantities are the energies of the ejected electrons. In this experiment only threshold photoelectrons ejected from ionisation events are detected. These threshold photoelectrons have near zero kinetic energy and so equation (2.1) can be reduced to that of equation (2.2).

$$E(M^{2+}) = h\nu - \phi_{DIP} \quad (2.2)$$

Therefore, this technique allows the energy selection of the dication by tuning the energy of the ionising photon. Synchrotron radiation from the Super-ACO storage ring facility was used as the source of tuneable light for these experiments.

2.2 Light source

The Super-ACO storage ring facility came on line in 1987 as a source of synchrotron radiation for experimental use. The acceleration of positrons within the storage ring supplies photons over the energy range from infrared to soft X-ray. The storage ring consists of 8 straight sections and 8 curved sections, which confine the accelerated positrons to a closed octagonal path. A linear accelerator injects the ring with 2 or 24 packets of positrons, which create a positron beam with lifetimes of about 5 or 10 hours respectively. The number of packets of positrons injected into the storage ring cause the light generated to have a time structure, which can be of experimental use. The 2 packet mode of the ring is used for timing experiments whereas the 24 packet mode provides a pseudo-continuous light source. The time of revolution of one packet of positrons within the ring is 240 ns. Therefore, the repetition rate of the generated light is 8.3 MHz and 100 MHz for the 2 packet and 24 packet mode respectively. The typical rate of quadruple coincidence detection is less than 1 Hz, as this is much lower than the repetition rate of the light incident on the source region both operational modes can be considered to give a continuous source of light for this experiment.

Synchrotron radiation is produced by the acceleration of charged particles through curved trajectories. The Super ACO storage ring uses both bending magnets and undulators to produce synchrotron radiation. Bending magnets accelerate the charged particles by changing their trajectory through a certain angle; the synchrotron radiation is then emitted tangentially to the circular path of the particles. Undulators consist of a series of periodically arranged magnets of alternating

polarity, which cause the beam to oscillate perpendicularly to its direction of motion. These oscillations produce synchrotron radiation emitted parallel to the beam.

2.3 Beamline

The Super-ACO storage ring has 25 beamlines, which guide the synchrotron radiation, generated by bending magnets and undulators, to experimental stations. This experiment was mounted on beamline SA31, which collects the light emitted by the positron beam passing through a bending magnet of the storage ring³. The beamline, shown schematically in figure 2.3.1, contains slits and mirrors to control the intensity and position of the photon beam and a grating monochromator to select the energy of the light. The first two mirrors in the beamline collect the light from the bending magnet and focus it onto the entrance slit. The next mirror reflects the light onto the monochromator, the energy selected light from the monochromator is then collected and focus onto the exit slit by a toroidal mirror. A final mirror is then used to focus the light into the source region of the experiment.

This beamline has three interchangeable plane grating monochromators, which are optimised for the transmission of first order light over different range of energies, see table 2.3.1.

Grating	Lines/mm	Energy range (eV)
1	600	12-40
2	900	10-120
3	1800	100-250

Table 2.3.1 Details of the three interchangeable plane gratings installed on beamline SA31.³

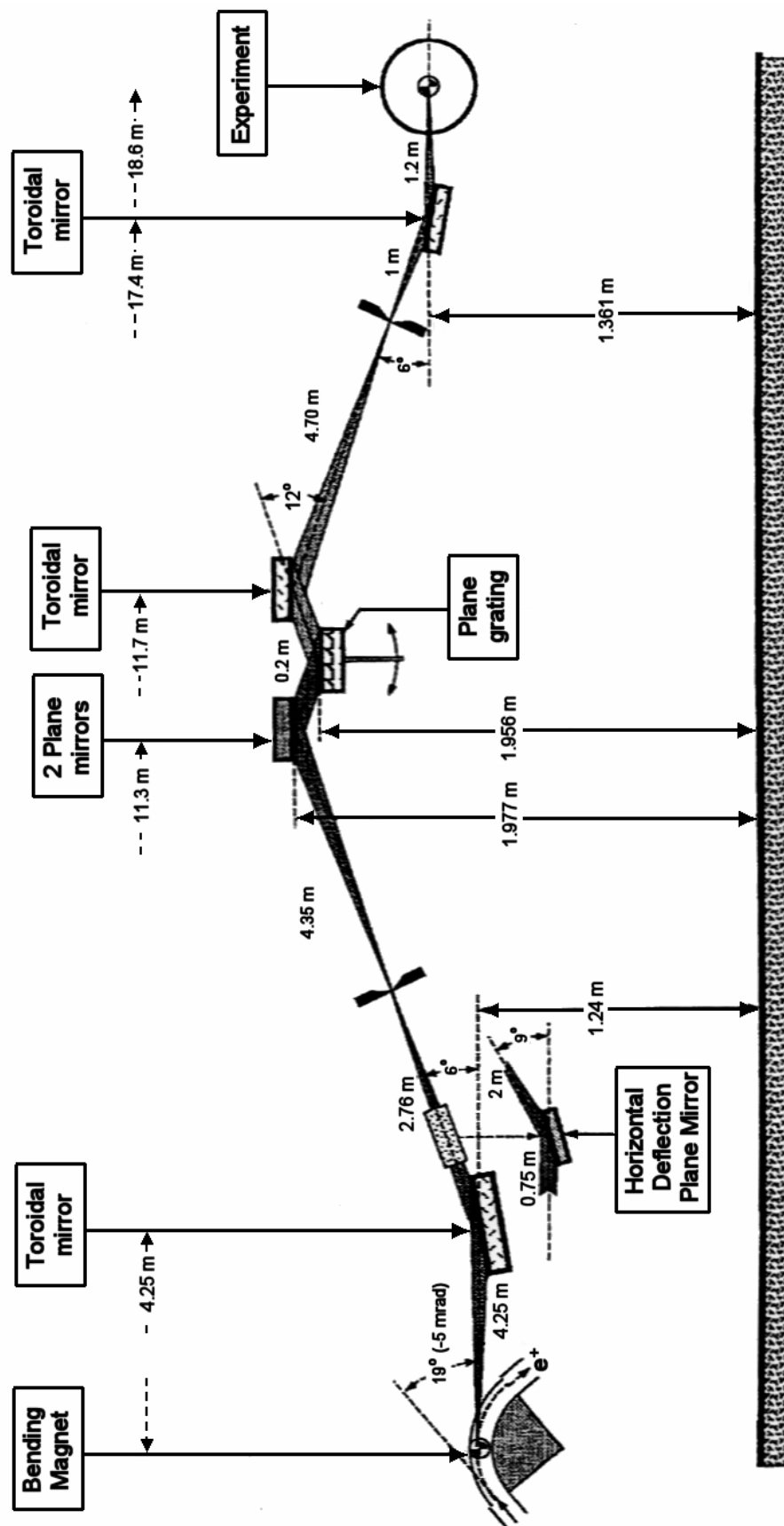


Figure 2.3.1 Schematic diagram of beamline SA31.3. The light generated by the positrons passing through the bending magnetic is focused on to a plane grating by a series of mirrors. The light is then energy selected and focused into the experimental source region by another set of mirrors.

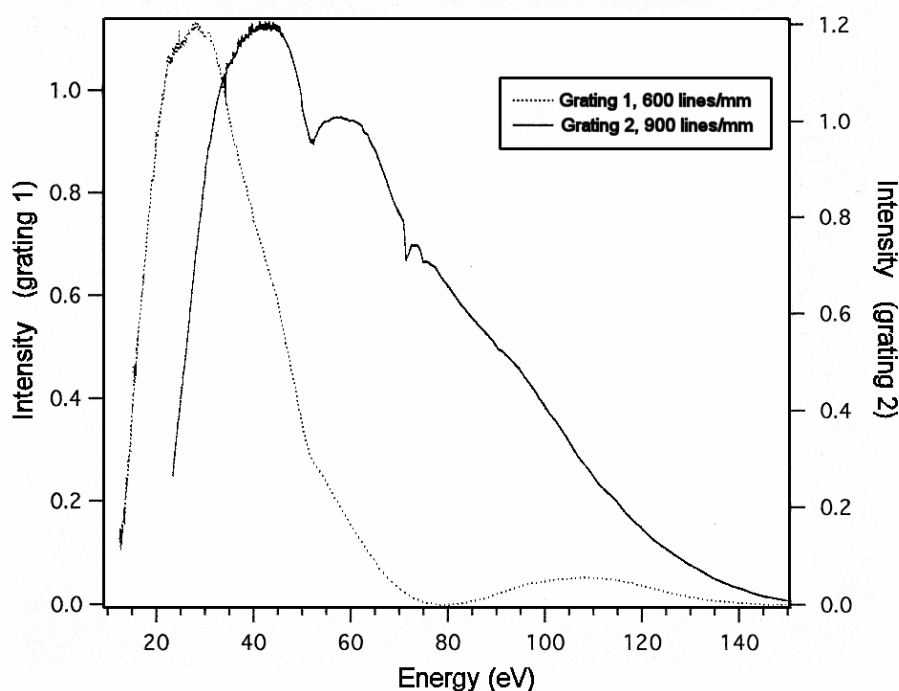


Figure 2.3.2 The intensity of first order light transmitted for gratings 1 and 2 as a function of energy.

Several molecular species were investigated with the use of this experimental method. The double ionisation energies for these molecules differ, therefore a grating was used which provided the greatest photon intensity over the required ionisation range. Figure 2.3.2 show the transmission functions for both gratings 1 and 2. Grating 1 provides the most photon flux over the energy range 20-35 eV and so this grating was used to provide light for the double ionisation of molecules over this range, such as C_6H_6 . At the higher photon energies range, 30-50 eV, the photon intensity from grating 1 drops, however, the intensity of grating 2 is high over this energy range. Therefore, grating 2 was used to select the energy of the photons for this higher energy range and used for the ionisation of CO_2 molecules. When using grating 2 an aluminium filter was placed within the beamline to remove second order light from the photon beam. An aluminium filter was used as aluminium strongly absorbs photons above 72 eV in energy and so effectively removes second order light from selected photon energies between 36 and 72 eV.

2.4 Apparatus

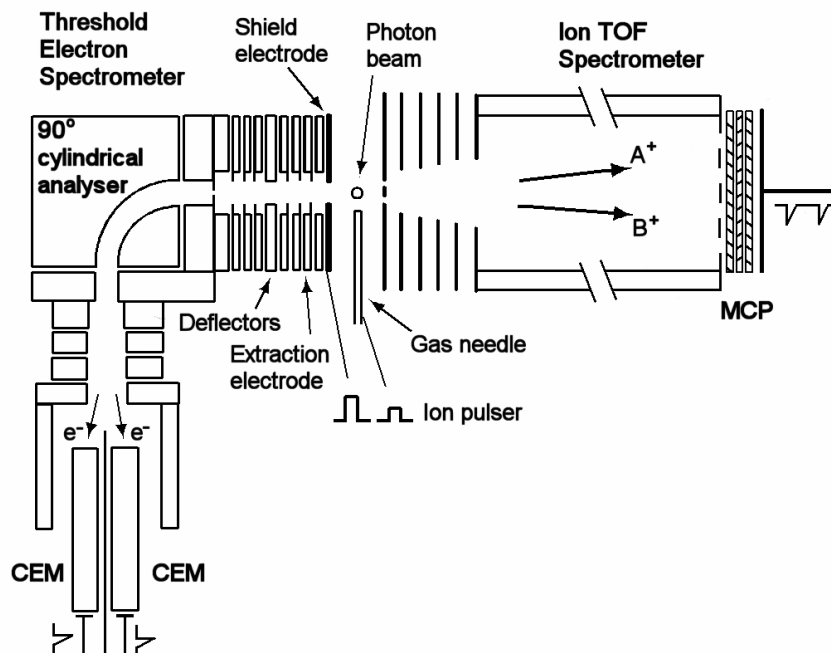


Figure 2.4.1 Diagram of experimental apparatus used for the collection of coincidence data, taken from reference 1.

The coincidence spectrometer used in this study is shown schematically in figure 2.4.1. Neutral molecules were introduced through a hypodermic needle into the common source region of the photoelectron and mass spectrometers. This effusive molecular gas jet was crossed perpendicularly with the photon beam from the beamline to produce molecular ions. Threshold electrons were extracted from the interaction region using the penetrating field technique,^{1,4} energy selected and then detected using four channeltron detectors. The detection of threshold electrons triggered an extraction pulse within the source region that pushed any ions present into the time of flight spectrometer. The times-of-flight of the ions were measured with a time-to-digital converter, TDC, card mounted inside an online computer. It was only possible to record the times-of-flight of up to three ions following each extraction pulse. Ion extraction pulses were triggered by the detection of one electron, two electrons or by random pulses provided by a pulse generator. Coincidence measurements were then made between one or two threshold electrons

or random pulses with up to three ions. The coincidences triggered by one electron and random pulses were required for the removal of false coincidences from the spectra triggered by electrons pairs. The acquisition time and number of events that trigger the extraction pulse for each spectrum were also recorded for use in the removal of false coincidences.

2.5 Threshold electron detection and TPEsCO spectrometry

The collection of ‘zero’ energy or threshold electron pairs in coincidence allows the internal energy of dications to be selected by tuning the photon energy, see section 2.1. A high electron collection efficiency is required as only a fraction of the electrons ejected in multiple ionisation events are threshold electrons. In this experiment the Penetrating Field Technique, PFT,^{1,4} was used to collect threshold electrons over 4π steradians within the source region. In this method a field generated by an extraction electrode is applied to the source region through a grounded shield. This field creates a shallow potential, which guides threshold electrons into an electron spectrometer. The electron spectrometer consists of a lens stack followed by an energy analyser and electron detectors. Energetic electrons ejected towards the lens stack are collected along with the threshold electrons guided by the penetrating field. The collection of energetic electrons results in a high energy tail to the distribution of electrons entering the spectrometer. The 90° cylindrical analyser was used to energy select the threshold electrons and remove the high energy tail from the distribution.

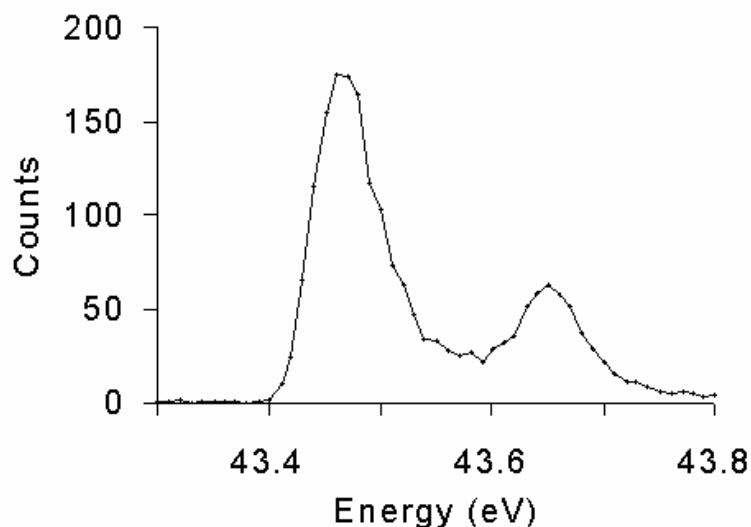


Figure 2.5.1 Graph showing the TPESCO spectrum of the ground state of the argon dication, $\text{Ar}^{2+} 3p^4 (^3P)$.

The threshold electrons were then detected by a set of four Channel Electron Multipliers, CEMs. A single CEM cannot detect multiple electrons simultaneously, so an array of four CEMs were used to allow the detection of pairs of threshold electrons in coincidence. Figure 2.5.1 shows the TPESCO spectra for the $3p^4 (^3P)$ double ionisation features of argon.^{5,6} These ionisation features along with the $\text{Ar}^+ 3s^{-1}$ and $\text{Ar}^{2+} 3s3p^5 (^3P)$ features were used to calibrate the energy of the photons selected with the monochromator.

2.6 Time of flight mass spectrometer

The times-of-flight of the dications and ion fragments formed by photoionisation were measured with the use of a Wiley-McLaren type two-field time-of-flight mass spectrometer. A schematic diagram of the two field TOF spectrometer is shown in figure 2.6.1.

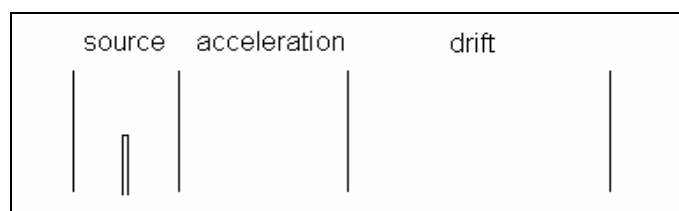


Figure 2.6.1 Schematic diagram of a two field TOF mass spectrometer.

The spectrometer has two electric field regions, the source and acceleration regions followed by a field free drift region. The electric fields are applied to the regions of the spectrometers with voltage ‘plates’, composed of mesh grids, which allow the transmission of ions from one region to the next. The grids have a transmission efficiency of 90%. The separation of the voltage plates in the spectrometer was designed to allow second order space focusing.⁷ This compensates for small variations in the initial position of the ions and minimises the variation in the times-of-flight due to the initial position of the ions. This focusing technique also causes the times-of-flight to become linearly dependent on the initial momentum of the ions.

2.7 Data collection methods

Two methods of data collection were used for this experiment. Initially the computer interface for the experiment only allowed the collection of up to three ions following a trigger event. As a consequence of this the ion count rate during the experiments were decreased so that the number of higher order ion event, those where more than three ions are produced following a pulse, were reduced. The ion count rate was reduced so that the number of triple ion events were of the order of 10% of the number of single ions detected, so that the number of quadruple and higher ions became negligible.

The range of times-of-flight recorded could be controlled by the electronics so that measurements begin after a certain time delay following a trigger pulse and

stop after a suitable time window. This introduced a time-of-flight offset as the ion flight times were measured from the end of the delay.

A later development of the experiment involved a more comprehensive computer interface, which allowed the detection of multiple ions, up to 16 ions, following a trigger event and within a fixed time-of-flight window. This new method also allowed the simultaneous measurement of the 1e, 2e and pulse triggered spectra.

2.8 References

- ¹ Penent F., Hall R.I., Panajotovic R., Eland J.H.D., Chaplier G., Lablanquie P., *Phys. Rev. Lett.*, **81** (1998) 3619
- ² Hall R.I., McConkey A., Ellis K., Dawber G., Avaldi L., MacDonald M.A., King G.C., *Meas. Sci. Technol.*, **3** (1992) 316
- ³ Thomas D., Coville M., Thissen R., Morin P., *Synchrotron Radiat. News*, **5** (1992) 8
- ⁴ Cvejanovic S., Read F.H., *J. Phys. B: At. Mol. Phys.*, **7** (1974) 1180
- ⁵ Avaldi L., Dawber G., Gulley N., Rojas H., King G.C., Hall R., Stuhec M., Zitnik M., *J. Phys. B: At. Mol. Opt. Phys.* **30** (1997) 5197
- ⁶ Martin, W.C., Fuhr, J.R., Kelleher, D.E., Musgrove, A., Podobedova, L., Reader, J., Saloman, E.B., Sansonetti, C.J., Wiese, W.L., Mohr, P.J., and Olsen, K. (1999). *NIST Atomic Spectra Database* (version 2.0), National Institute of Standards and Technology, Gaithersburg, MD (<http://physics.nist.gov/asd>), November 2003
- ⁷ Eland J.H.D., *Meas. Sci. Technol.*, **4** (1993) 1522